JRMP Journal of Radiopharmaceuticals and Molecular Probes Vol. 1, No. 1, 2015
J Radiopharm Mol Probes 2015;1(1):62-73
ISSN 2384-1583

ORIGINAL ARTICLE

Sentinel lymph node mapping using tri-modal human serum albumin conjugated with visible dye, near infrared fluorescent dye and radioisotope

Se Hun Kang[1], Seo-il Kim[1], So-Youn Jung[2], Seeyoun Lee[2], Seok Won Kim[2], and Seok-ki Kim[1,2,*]

[1]Molecular Imaging and Therapy Branch, Research Institute and Hospital, National Cancer Center; [2]Center for Breast Cancer, Research Institute and Hospital, National Cancer Center, Goyang, Korea

ABSTRACT

We developed an evans blue-indocyanine green-^{99m}Tc-human serum albumin conjugate for sentinel lymph node mapping and we describe its unique potential usage for clinical implications. This conjugate has combined the strengths of visible blue dye, near-infrared fluorescence and radioisotope into one single conjugate without any additional weakness/disadvantage. All the components of evans blue-indocyanine green-^{99m}Tc-human serum albumin are safe and of low cost, and they have already been clinically used. This conjugate was stable in the serum, it showed a long retention time in the lymphatic system and the lymph nodes showed a much higher signal-to-noise ratio after the conjugate was injected intradermally into the paw of mice. Both the single-photon emission computed tomography and near-infrared fluorescent images of the mice were successfully obtained at the same time as the excised sentinel lymph nodes showed blue color. The visual color, near-infrared fluorescence and gamma ray from this agent could be complementary for each other in all the steps of sentinel lymph node sampling: exploring and planning sentinel lymph node before excision with visualization of the exact sentinel lymph node location during an operation. Therefore, the triple modal agent will possibly be very ideal for sentinel lymph node mapping because of the high signal-to-noise ratio for non-invasive imaging and its complementary multimodal nature, easy preparation and safety. It is promising for clinical applications and it may have great advantages over the traditional single modal methods.
J Radiopharm Mol Probes 1(1):62-73, 2015

Key Words: Triple modal imaging, Sentinel lymph node (SLN), Near-infrared fluorescent imaging (NIRF), SPECT imaging

Introduction

Sentinel lymph node (SLN) sampling is accepted as a standard procedure for early stage breast cancer (1-4). The accuracy and ease of the procedure largely depend on the SLN mapping agents, and many important aspects are related to their use: safety for human application, the imaging or detecting methods for the radiation, dye and fluorescence, the operator's ability and the required apparatus for the materials' disposal (5-10). Although a SLN sampling procedure is a relatively simple operation, the extent of this surgery has to be decreased to as small as possible (a so-called "pinpoint operation") (11). Because of these practical requirements, SLN mapping needs to be planned before the operation.

SLN mapping has been carried out using various agents such as visual dye, fluorescent dye and radioactive agents. Among them, gamma imaging (e.g. SPECT) is a clinically mature technique. It is the most practical non-invasive

Received February 16, 2015 / Revised March 31, 2015 / Accepted April 2, 2015

Corresponding Autor: Seok-ki Kim, M.D., Ph.D.
Research Institute and Hospital, National Cancer Center, 323 Ilsan-ro, Ilsandong-gu, Goyang 410-769, Korea
Tel: +82-31-920-1731, Fax: +82-31-920-2630, E-mail: skkim@ncc.re.kr

imaging as it has the most powerful penetration power and a high signal to background ratio. Radiolabeled colloids such as ^{99m}Tc-sulfur colloids are very stable in the living body and their retention time in a SLN is relatively long (12). However, this imaging method requires rather expensive equipment that is often not available in an operation room. Fluorescent imaging is an effective process, yet its penetration is not good as gamma imaging, but it can visualize shallowly located organs such as an axillary SLN, and especially when using near-infrared fluorescence (NIRF). NIRF agents hold great promise for non-invasive in vivo imaging due to the low tissue auto-fluorescence and relatively deep tissue penetration in this region of the electromagnetic spectrum (13-15). But this imaging system is still difficult to be used in the operation room, although it is less expensive than a gamma camera. On the other hand, in the operation room, visual dye is so favorable to guide a surgeon. During the operation it visually stains the target tissues, which can be harvested easily by a simple surgical procedure rather than performing noninvasive targeting before making an incision (15). Using gamma and/or NIRF imaging, SLN sampling can be done more precisely, but it is better if the operator is directly guided during operation, which means that a visible function of the targeting agent is very helpful for the operator. Even so, dye is not optimal for SLN targeting because its size is too small to reside very long in the SLN during the operation.

From the practical point of view, a SLN mapping procedure requires many steps before an operation and during surgical exploration, and each imaging step requires different characteristics from the SLN targeting agents. For example, pre-imaging of radioactive or fluorescent agents helps to perform an accurate operation, while a visual staining agent is still more advantageous for the surgical exploration step. So, we can identify the exact location of a SLN before an operation by using non-invasive imaging methods, followed by staining a SLN with visual dye to take it out during the surgical procedure. Using these characteristics, we can minimally incise non-target tissues, pick out only the SLN and decrease the damage to the normal tissue, as well as reduce the subsequent complication.

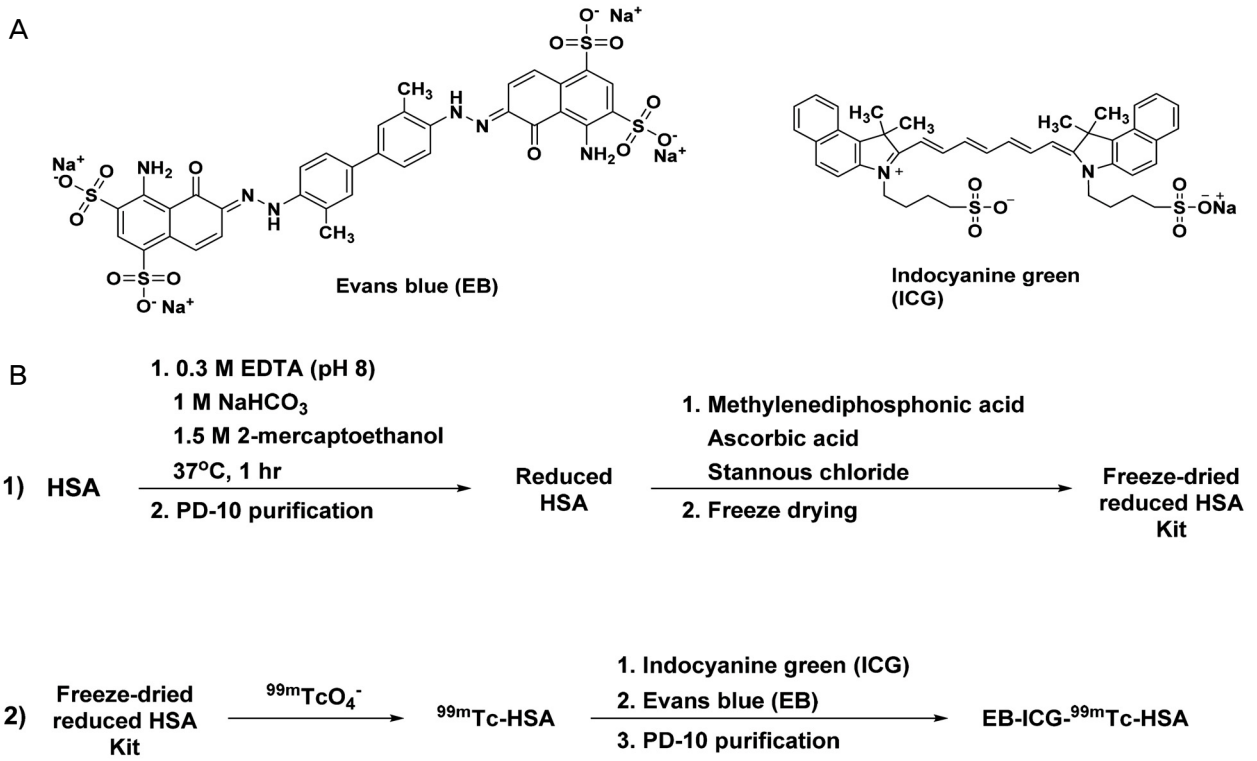

Scheme 1. Schematic chemical structure and preparation schemes of EB-ICG-^{99m}Tc-HSA. (A) The chemical structures of Evans blue (EB) and indocyanine green (ICG). (B) Preparation schemes of EB-ICG-^{99m}Tc-HSA.

Consequently, the development of multimodal agents will help performing precise SLN mapping and surgical procedures, so we prepared a tri-modal human serum albumin (HSA)-based agent conjugated with a visible dye (Evans blue; EB), a near infrared fluorescent dye (Indocyanine green; ICG) and a radioisotope (^{99m}Tc), and all these components are safe and they have already been used clinically (Scheme 1A). For clinical application, this conjugate was analyzed for its in vivo stability, characteristics and in vivo usage, and we also performed acute toxicity tests.

Materials and Methods

1. Materials and instruments

The solvents and liquid reagents were transferred using hypodermic syringes and micro pipettes and all the glassware was dried in an oven at 150 °C prior to use. Twenty percent human serum albumin (HSA) was purchased from SK Chemical and ^{99m}Tc-pertechnetate was eluted from an Ultra-Technekow™ DTE generator (Mallinckrodt Pharmaceuticals, Dublin, Ireland) for radiolabeling. A Sephadex G-25 (PD-10) column (GE Healthcare Life Sciences, Pennsylvania, USA) was used for purification. A BCA™ protein assay kit and Ellman's reagent were purchased from Pierce (Illinois, USA). All the other reagents and solvents used were reagent grade and they purchased from Sigma-Aldrich (Seoul, Korea). The thin layer chromatography was scanned using an AR-2000 radio-TLC Imaging Scanner (Bioscan, Washington, D.C., USA) and the NIR signals were measured by a Safire2 microplate reader (Tecan, Männedorf, Switzerland). The size of the conjugate was checked using a Zetasizer nano ZS (Malvern Instruments Ltd, Malvern, UK). A NanoSPECT (Bioscan, Washington, D.C., USA) was used for the animal in vivo SPECT imaging, and the NIRF images and biodistribution data were obtained using an IVIS Lumina imaging system (Caliper Life Sciences, Massachusetts, USA). All the photographs were taken by a digital camera called a Power Shot G9 (Canon, Tokyo, Japan). The harvested SLN sections were examined by a Leica DMD108 light microscope (Leica, Wetzlar, Germany). A Wizard gamma counter (Perkin Elmer, Massachusetts, USA) was used to obtain the gamma biodistribution data.

2. Optimal concentration screening of EB-ICG-HSA in vitro and in vivo

To identify the optimal concentration of EB-ICG-HSA that shows the maximum NIRF intensity with a visible blue color, we screened the concentrations in three steps: 1) ICG concentration optimization, 2) concentration screening of the HSA conjugated with the optimized ICG and 3) concentration screening of the EB conjugated with the optimized ICG-HSA. First, 0.020-0.030 mM of ICG solution in distilled water were prepared in the dark, and the NIRF emission signal intensities of these samples were screened at 760 nm for excitation and 810 nm for emission by using a Safire2 micro plate reader (n=3). The ICG-HSA was secondly screened in the range of 0.060-0.30 mM of HSA with the optimized ICG concentration (n=3). Last, the EB concentration with the optimized ICG-HSA was also searched in the range of 0.0050-1.30 mM of EB (n=3).

For the optimal in vivo fluorescence imaging, the NIRF signal intensity that varied with the concentration changes of EB-ICG-HSA was measured in 10 week old BALB/c mice. First, 0.1, 1 and 10 times concentrated solutions, as compared with that of the optimal EB-ICG-HSA (in vitro) were prepared, and the mice were intradermally injected with 50 μL of each of the prepared samples into the second dorsal toe of the both hind paws, and all the NIRF images were obtained using an IVIS Lumina imaging system equipped with a NIRF filter set (excitation/emission, 705-780/810-885 nm) at 1 hr post injection. To make sure of obtaining the NIRF and visible results, the skin of the legs was striped above the ankles.

3. Radiolabeling, dye conjugation and characterization of EB-ICG-^{99m}Tc-HSA

For ^{99m}Tc radiolabeling, the reduction of disulfide groups in the HSA was done as is shown in scheme 1B, and this was based on a previously described procedure (16). Briefly, 400 μL of 0.3 M ethylenediaminetetraacetic acid (EDTA, pH 8), 400 μL of 1 M $NaHCO_3$ and 500 μL of 1.5 M 2-mercaptoethanol were added to the 600 μL (120 mg) of 20% HSA solution diluted to a total volume of 2.5 mL using 0.1 M Na_2CO_3. The mixed solution was incubated at 37 °C for 1 hr to reduce the disulfide to thiol groups in the HSA, and the

crude product was purified with a PD-10 column and using phosphate-buffered saline (PBS) (pH 6). The obtained reduced HSA fraction was transferred to a glass vial and this was followed by adding methylenediphosphonic acid 0.17 mg, ascorbic acid 3.7 μg and stannous chloride 8.45 μg. The glass vial was frozen at -80°C for 24 hrs and then this was freeze dried. The quantitation of the prepared reduced HSA was assayed with a BCA™ protein assay kit (17) and the number of free thiol groups in the reduced HSA was measured using Elman's reagent (16). One mL of the 370 MBq of $^{99m}TcO_4^-$ eluted from an Ultra-Technekow™ DTE generator was added to the freeze-dried reduced HSA vial, and the vial was incubated at room temperature for 10 min. The radiolabeling efficiencies were checked by performing both ITLC (ethanol:10% ammonium acetate=1:1) and 5% bovine serum albumin (BSA)-impregnated paper chromatography (saline).

For dye conjugation, ICG 0.21 mg was first added to ^{99m}Tc-HSA, and the mixture was shaken at room temperature for 30 min in the dark. EB 8.5 mg was added to the mixed ICG-^{99m}Tc-HSA and this was shaken at room temperature for 60 min in the dark. After finishing all the conjugation steps, the final product was purified with a PD-10 column. The collected dark blue fraction was evaporated and diluted to a total volume of 1 mL using 0.05 M PBS (pH 7.4). To confirm the preparation of EB-ICG-^{99m}Tc-HSA, ITLC was again performed, and the resultant size of the conjugate was measured using a Zetasizer nano ZS. Its radiochemical stability in human serum was screened up to 24 hrs (n=3).

4. In vivo animal SPECT, NIRF and visible imaging

For animal imaging, we used twelve BALB/c-nu mice that were over 10 weeks old. Anesthesia was done using 2% isoflurane in 100% oxygen. EB-ICG-^{99m}Tc-HSA 18.5 MBq/50 μL were intradermally injected into the second dorsal toe of both hind paws with the needle pointed in a rostral direction after warming the paws by warm water, and then the injection sites were pressed for about 1 min to facilitate the dye's uptake and movement through the lymphatic vessels. One hour after injection, the SPECT image was scanned. The animal SPECT scan was performed in a helical scan mode of NanoSPECT. It was acquired for 10 min, and the obtained image was reconstructed with the HiSPECT NG-Standard mode using a HiSPECT scientific visualizer. InVivoScope (Bioscan, USA) was used as the image processing and analyzing software. Also, the NIRF images were obtained using an IVIS Lumina imaging system equipped with a NIRF filter set (excitation/emission: 705-780/810-885 nm) at 1 hr post injection. The NIRF images were captured before/after the skin of the legs was striped above the ankles. The camera settings included the maximum gain, 2 × 2 binning, 1024 × 1024 pixel resolutions, a 10 cm field of view in diameter and 1 second exposing time. For the visible imaging, photographs were taken by a digital camera before and after the skin of the legs was striped above the ankle. All the animal protocols were in accordance with the 'Animal Care and Use Committee Guidelines' of our institution.

5. Histopathologic staining

After mice imaging of EB-ICG-^{99m}Tc-HSA, the blue dye labeled SLNs were excised from the lymph node basin. Half of the harvested tissues were fixed in 10% neutral buffered formalin for 1 day and then the tissues were dehydrated using 70% ethanol and next they were embedded in paraffin. Hematoxylin and eosin (H&E) staining was performed on the tissue section (5 μm thick). The rest of the tissues were embedded directly into optimum cutting temperature compound in dry-ice, and the frozen tissues were sectioned with a thickness of 30 μm. All the sections were examined using a Leica DMD108 light microscope.

6. Biodistribution studies

To obtain the biodistribution data of EB-ICG-^{99m}Tc-HSA, BALB/c mice over 10 weeks old were used (n=3). The injection condition was identical to the imaging protocols except only the right hind paws were injected. The mice were sacrificed at 60 min post injection, and the 13 organs (brain, blood, heart, lung, liver, spleen, kidney, stomach, intestine, femur, muscle, lymph node and foot) were collected, weighed and gamma counted. The percentage of the injected dose per organ (% ID/g) was calculated. The NIR fluorescence of the organ specimens were also measured using an IVIS lumina system. All the fluorescence signals were calculated by drawing ROIs covering each specimen. The total amount of

fluorescence was normalized in terms of the weight of the specimen (p/sec/cm^2/sr/g).

7. Acute toxicity tests

Luciferase expressing DRO cell lines were used for determining the cellular toxicity of EB-ICG-^{99m}Tc-HSA in vitro (n=3). They were prepared at 1 x 104 cells/100 μL/well on a 96-well plate. After EB-ICG-^{99m}Tc-HSA was added as 3, 0.3, 0.03 nmole, the cell lines were maintained up to 5 hrs. After washing three times with PBS, the cells were counted using a Cell Counting Kit-8 according to the manufacturer's recommendations. To determine the acute toxicity of EB-ICG-^{99m}Tc-HSA in small animals, BALB/c mice were used. The test group of mice was intravenously injected with 50 μL of a 10 times higher concentration than the optimal in vivo EB-ICG-^{99m}Tc-HSA concentration (n=5) whereas the control mice were intravenously injected with 50 μL of saline (n=5). The behavior and body weight change of mice were observed during 35 days. All the mice were sacrificed at the 35th day post-injection and the 6 tissues (lymph node, brain, heart, intestine, kidney and liver) were fixed in 10% formaldehyde, made into paraffin sections and stained with H&E for histological examination.

Results

1. Preparation of EB-ICG-^{99m}Tc-HSA

The optimal ICG concentration in distilled water was 0.027 mM (Figure 1A). Also, 0.18 mM of HSA conjugated to 0.027 mM of ICG showed the highest NIRF intensities (Figure 1B). With this result, the EB concentration for the EB-ICG-HSA conjugation was optimized as 0.88 mM (Figure 1C). Although, the NIRF intensity of EB-ICG-HSA showed higher results at a lower EB concentration, the blue color was not evident. For that reason, 0.88 mM of EB was chosen as being optimal in spite of this not showing the best results.

However, the NIRF signal of EB-ICG-HSA in vivo showed a different result. A 50 μL injection of a 10 times

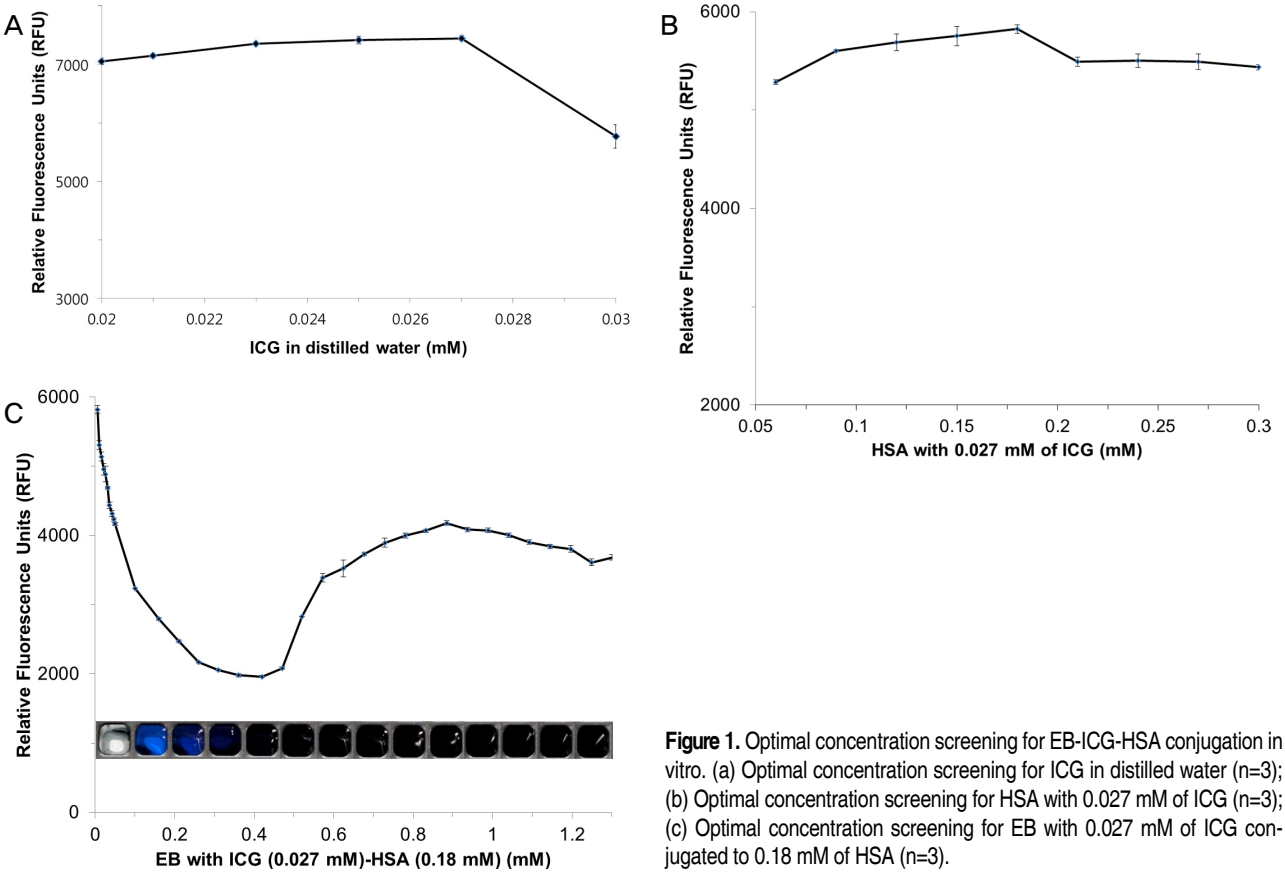

Figure 1. Optimal concentration screening for EB-ICG-HSA conjugation in vitro. (a) Optimal concentration screening for ICG in distilled water (n=3); (b) Optimal concentration screening for HSA with 0.027 mM of ICG (n=3); (c) Optimal concentration screening for EB with 0.027 mM of ICG conjugated to 0.18 mM of HSA (n=3).

higher concentration of EB-ICG-HSA showed the most intense result in the BALB/c mice since it was probably diluted inside the body (Figure 2). Therefore, the final composition of EB-ICG-HSA for 50 μL intradermal injection was 440, 13.5 and 90 nmole, respectively.

For ^{99m}Tc radiolabeling, the preparation yield of the reduced HSA was 91.8%. In the freeze-dried HSA, the number of reduced free thiol groups was 19.1 per HSA, which means that about four ^{99m}Tc are conjugated to a HSA molecule because four thiols are coordinated to one reduced ^{99m}Tc. After ^{99m}Tc labeling and the dye conjugation step, the size of EB-ICG-^{99m}Tc-HSA was measured as 32.22 nm. Both the ^{99m}Tc labeling efficiencies of ^{99m}Tc-HSA and EB-ICG-^{99m}Tc-HSA were over 99%. Moreover, EB-ICG-^{99m}Tc-HSA showed the high radiochemical stabilities in human serum for 24 hrs. Starting as 99.8±0.1% at 1 hr, the stability was maintained as 97.9±0.1% for up to 24 hrs (n=3) (Figure 3).

2. In vivo SLN identification by triple modal imaging and histopathological staining

Using EB-ICG-^{99m}Tc-HSA, the SLN was visualized by SPECT, NIRF imaging and it was observed with the naked eye during the SLN sampling operation. First, SPECT showed the exact location of the SLN on the 3 dimensional images without an invasive procedure such as skin incision or removal of tissues overlying the SLN (Figure 4B). NIRF imaging was done before/during the operation using a NIR camera and this also depicted the SLN (Figure 4C). In addition, the blue stained SLN was definitely observed after peeling the skin of the leg, and this visually depicted SLN was photographed (Figure 4D).

After triple modal imaging of 12 mice, all 40 blue colored lymph nodes were surgically harvested and all of them were radioactive, fluorescent and blue colored. The harvested tissues emitted both gamma-rays and NIR fluorescence as well as their color was definitely blue, which was clearly distinguished from the non-SLN tissue. All the harvested tis-

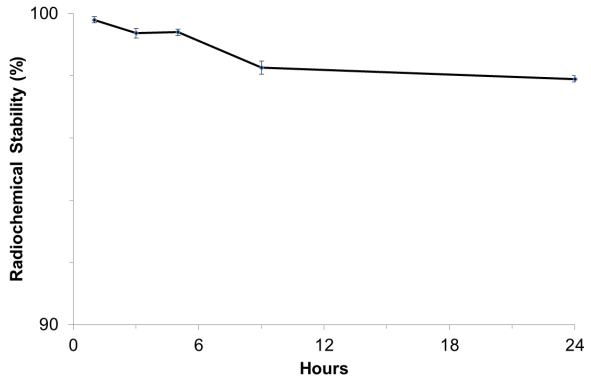

Figure 3. Radiochemical stabilities of EB-ICG-^{99m}Tc-HSA in human serum. EB-ICG-^{99m}Tc-HSA showed high radiochemical stability in human serum for 24 hrs. Starting as 99.8±0.1% at 1 hr, the stability was maintained as 97.9±0.1% for up to 24 hrs (n=3).

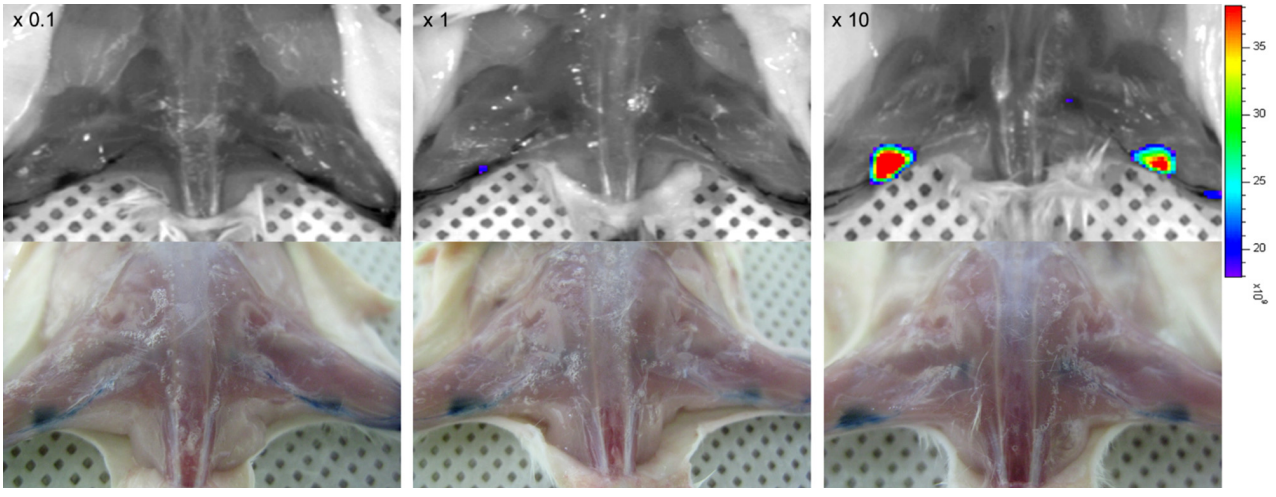

Figure 2. Optimal concentration screening for EB-ICG-HSA conjugation in vivo. The NIRF signal intensity, which varied with the concentration changes of EB-ICG-HSA, was measured by an IVIS Lumina optical imaging system and using 10 week old BALB/c mice. Among the 0.1, 1 and 10 times concentrated solutions of the optimal EB-ICG-HSA (in vitro), the 10 times higher concentration showed the highest intensity (excitation/emission, 705-780/810-885 nm) at 1 hr post-injection (top). All the lymphatic flow and nodes were also visible as blue (bottom).

sues on H&E staining were confirmed as SLNs, and the blue color was verified in the periphery of the frozen sections of the lymph nodes (Figure 4E).

3. Biodistribution studies

The biodistribution result of EB-ICG-^{99m}Tc-HSA in terms of ^{99m}Tc is displayed in Figure 5A. The uptake value of the SLNs was nearly 6 x 104 times higher than that of blood; meanwhile, all the other organs, except the injection site (foot), showed significantly low uptakes. The peak biodistribution result was seen at the popliteal lymph node and it reached 115.0±38.2 %ID/g, which was even higher than the injection site (46.6±11.5 %ID/g). Consequently, nearly all the radioactivity was distributed in just the lymph nodes. For the fluorescence, the NIRF showed high signals in the nodes and injection sites, while the liver and intestine also showed weak NIRF signals (Figure 5B,C).

4. Acute toxicity tests

On the cellular toxicity study, the viability of the DRO cells was not different according to the various concentrations (n=3, Figure 6A). On the acute toxicity test of EB-ICG-^{99m}Tc-HSA for 35 days, no significant difference of the test group was observed as to the control group (Figure 6B). The H&E staining results also showed no significant dissimilarity on comparison (Figure 6C).

Discussion

To develop an ideal sentinel lymph node imaging agent for clinical application, at least the following general criteria should be considered: 1) safety without acute systemic toxicity for clinically use, 2) deep tissue penetration for non-invasive imaging, 3) highly selective sentinel lymph node mapping by non-invasive imaging as well as visible dye staining for the surgical operation and 4) long retention at the target site to acquire a high signal-to-noise ratio. These practical issues are not trivial in clinical terms. Standard techniques for sentinel lymph node biopsy (SLNB) include radioisotopes, visual dye, and a combination of both. However, these conventional techniques have certain limitations. Although visual blue dye can show the SLN directly by the dye color, it

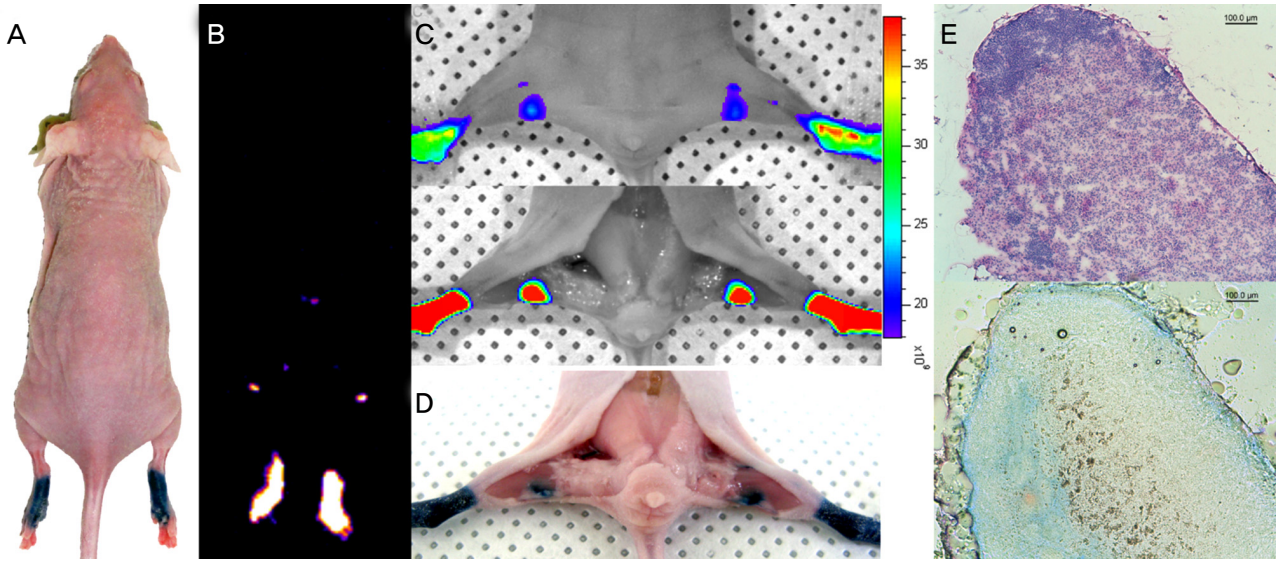

Figure 4. In vivo sentinel lymph node mapping using tri-modal imaging of EB-ICG-^{99m}Tc-HSA and histopathological staining. Intradermal injections were done with 18.5 MBq/50 μL of EB-ICG-^{99m}Tc-HSA into the both hind paws of the BALB/c-nu mice, and all the images were obtained 1 hr post-injection. (A) Color image of a BALB/c-nu mouse; (B) Non-invasive in vivo SPECT SLN image of the mouse; (C) Non-invasive in vivo NIRF SLN images before (top)/after (bottom) the skin of the legs was striped (excitation/emission: 705-780/810-885 nm); (D) The in vivo visible SLN image is seen as blue; (E) The H&E stain image verified that the SLN was precisely harvested as guided by the triple modal conjugate (top). The microscope image showed the blue stained SLN features by EB-ICG-^{99m}Tc-HSA (bottom).

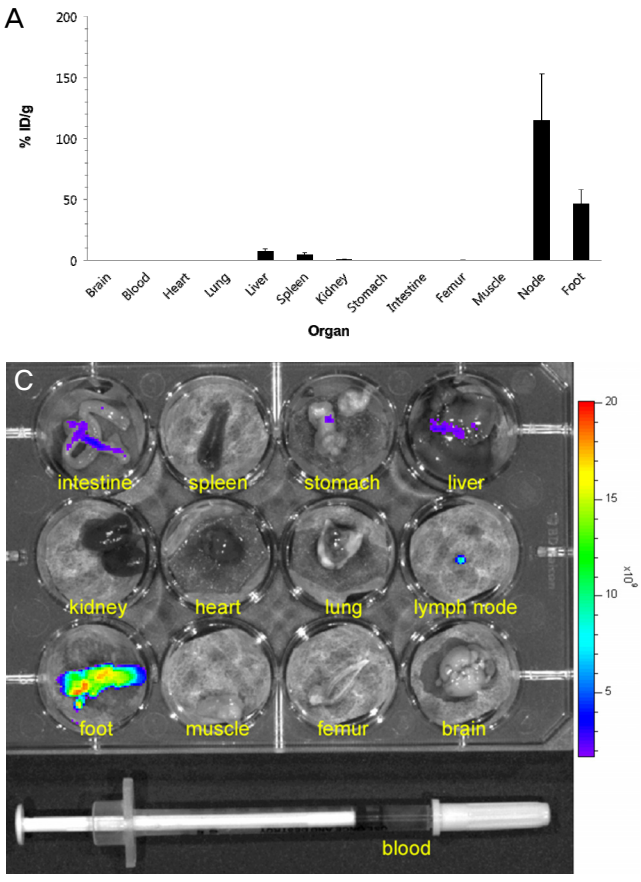

Figure 5. Gamma and NIRF biodistribution results of EB-ICG-^{99m}Tc-HSA in BALB/c mice (n=3). Intradermal injections were done with 18.5 MBq/50 μL of EB-ICG-^{99m}Tc-HSA into the right hind paws of the mice. All the mice were sacrificed at 1 hr post injection, and the 13 organs (brain, blood, heart, lung, liver, spleen, kidney, stomach, intestine, femur, muscle, lymph node and foot) were collected, weighed and gamma counted and NIRF imaged. (A) The data for gamma counting. The percentage of the injected dose per organ (%ID/g) was calculated. The lymph node reached 115.0±38.2 %ID/g, which was even higher than that at the injection site (46.6±11.5 %ID/g); (B) The NIRF statistical data. All the NIR fluorescence signals were calculated by drawing ROIs covering each specimen (p/sec/cm2/sr/g). The NIRF showed relatively high signals in the nodes and injection sites, although the liver and intestine also showed weak NIRF signals; (C) The NIRF image of each organ.

easily loses its visibility because of dense fat, intraoperative bleeding, or rapid transition (6,18). Consequently, the identification rate of SLNs by visual dye was only 70-80 %, lower than that by RI alone or the combination of both, and the addition of RI improved the detection rate (8,19-21). Moreover, visual dye cannot provide the location of the SLNs before skin incision because it cannot penetrate the dermis. Thus, inexperienced surgeons should make a long incision. The use of RI requires a high cost and a radioactive facility and has the risk of radiation exposure. In addition, the localization of SLNs by using a handheld gamma probe could be difficult because it is guided by sound and not by visualization (20). For that reason, multimodal signal emitting SLN agents are exceptionally advantageous for a surgeon when considering several aspects of SLN mapping. According to Morton (22) and Giuliano (23, 24), substantial experience, about 20 to 30 patients, is needed until the surgeon acquires the techniques. There is no doubt a multimodal agent could reduce this learning curve. Accordingly, we developed a new tri-modal imaging agent EB-ICG-^{99m}Tc-HSA in which all the components are safe, inexpensive and all of them have already been clinically used.

^{99m}Tc is one of the most widely used radioisotopes in medicine. Likewise, HSA, which is the most abundant protein in human blood plasma, has been used as the multifunctional platform for diagnosing and treatment such as drug delivery because it behaves like nanoparticles as a natural colloid and it has long history of human applications with good safety. As a NIRF dye, we adopted ICG. Inorganic quantum dots have recently shown unique optical properties among the various NIRF dyes, but their safety is still a serious concern since there are toxic elements in their cores (25, 26). ICG is approved for clinical use in hepatic function examinations and fluorescent angiography (27). ICG fluorescence imaging has recently been reported on for SLN mapping in cancer therapy (28,29). Actually, we wanted to find a NIRF dye that functions for visible imaging at the same time, yet ICG could not be used as a visible color dye

simultaneously because it typically does not show a strong green color when the NIRF is maximum. Thus, we included a visible dye (EB) in the SLN mapping conjugate. EB is an azo compound and it has weak fluorescence (excitation: 470 nm and 540 nm; emission: 680 nm). Although it can slightly emit fluorescence, its range is not NIR, so we used it only as visible blue color dye. It has also been used in human applications; it is useful in physiology for estimating the proportion of body water contained in blood plasma due to its high affinity for albumin, and it has been tested clinically in SLN mapping (30).

To develop EB-ICG-^{99m}Tc-HSA, we first screened the optimal ICG concentration in distilled water in vitro because the fluorescent signal intensity normally varies by its self-aggregated property; if its concentration is too high, then the fluorescent signal goes down by self-quenching. The optimized ICG concentration to show the highest NIRF signal was 0.027 mM (Figure 1A). On the base of this result, the HSA concentration in ICG-HSA was optimized as 0.18 mM (Figure 1B). Next, the EB concentration for the EB-ICG-HSA conjugation was screened and optimized as 0.88 mM (Figure 1C). Although the NIRF intensity of EB-ICG-HSA showed higher results at a lower concentration of EB (<0.005 mM), the blue color was not apparent enough for visible mapping. For that reason, 0.88 mM of EB, which showed evident blue color with a fairly high NIRF, was chosen as the optimal concentration, even though EB slightly quenched the ICG fluorescence. On the other hand, it is interesting that the NIRF signal of EB-ICG-HSA showed a different result in vivo. A 10 times higher concentration of EB-ICG-HSA injected to BALB/c mice showed the highest NIRF intensity (Figure 2). We assumed that this could be caused by dilution of the conjugate inside the body.

For SPECT imaging with EB-ICG-^{99m}Tc-HSA, a radioisotope must be introduced, so we modified the HSA structure for ^{99m}Tc labeling. To carry out ^{99m}Tc labeling, the disulfide groups in HSA had to be reduced to thiols (Scheme 1b). The number of reduced thiol groups was 19.1 per HSA, which explains that about four ^{99m}Tc are conjugated to a HSA molecule as four thiols are supposed to coordinate with one reduced $^{99m}TcO_2$. After finishing the radiolabeling, the NIRF and visible dye conjugation to HSA followed, as well as a purification step of EB-ICG-^{99m}Tc-HSA. From the point of view of radiochemistry, the prepared EB-ICG-^{99m}Tc-HSA showed not only high radiochemical purity, but also radiochemical stability in human serum for up to 24 hrs (Figure 3).

To perform in vivo SLN identification using EB-ICG-^{99m}Tc-HSA, non-invasive imaging and visible imaging were both done. Animal SPECT pointed out the exact location of the SLN in the mouse (Figure 4B). Plus, the NIRF imaging using the IVIS Lumina also non-invasively indicated the SLNs (Figure 4C). The NIRF signal of SLN was even observed before the skin of the legs was striped. To take out the SLN, we peeled the skin of the legs, and the blue stained SLNs were clearly observed and photographed (Figure 4D). In addition, 40 blue dye labeled lymph nodes were excised from the lymph node basin of 12 mice. The harvested blue tissues emitted gamma-ray and NIR fluorescence. The H&E staining results confirmed that the harvested tissues were SLNs, and the obtained blue SLNs were simple to distinguish from the non-SLN tissue (Figure 4E).

To statistically analyze body uptakes, 2 kinds of biodistribution studies were done. All the extracted 13 organs of all the mice were both gamma counted and fluorescently analyzed. From the gamma counting results, only the lymph nodes showed an extremely obvious %ID/g value (Figure 5A). On the other hand, the NIRF biodistribution data slightly differed from the gamma results, which additionally showed weak NIRF signals of the liver and intestine (Figure 5B,C). We assumed that this is because of a bit of ICG was released from the HSA, and this could be explained by the way ICG was conjugated to HSA. The chemical structure of ICG is not suitable for making a covalent bond, and the ICG was noncovalently bound with HSA. Because of the negatively charged polymethine structure, ICG noncovalently interacts with various proteins. Even if noncovalent bonding is considerably less stable than covalent bonding, it makes a faster rate of conjugation even in a mild condition. In addition, if we wanted to make a covalent bond, then modifying the ICG structure would be inevitable, which means that we cannot sure of the toxicity of a newly changed structure of ICG inside a body. ICG-HSA complex has already been noncovalently prepared (31). Likewise, we noncovalently conjugated ICG to HSA, although a bit of ICG was released from the HSA.

For clinical application, we performed acute toxicity tests.

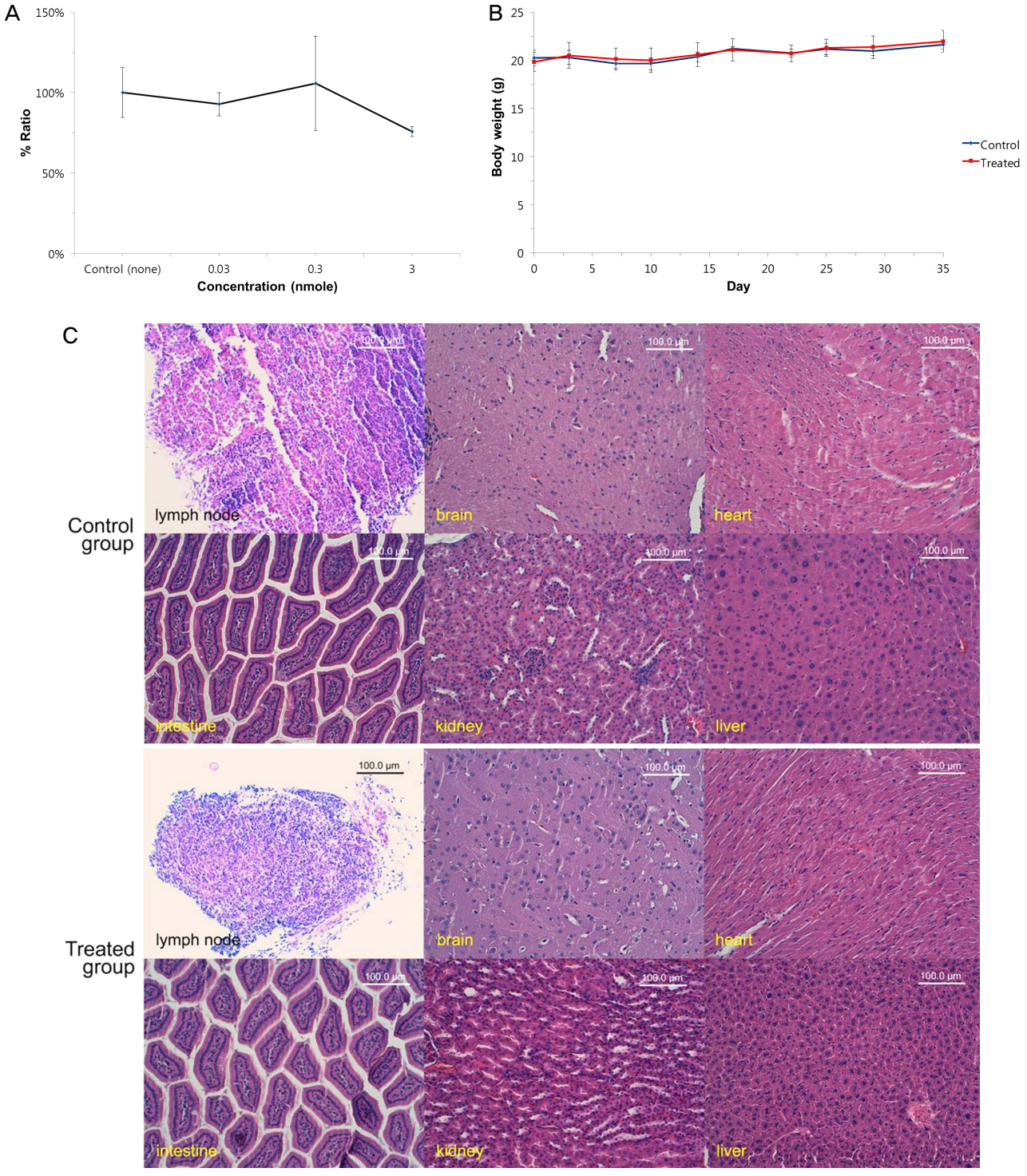

Figure 6. Acute toxicity test results. (A) Assays for the cellular toxicity of EB-ICG-^{99m}Tc-HSA (n=3). Luciferase expressing DRO cell lines were prepared with 1 x 104 cells/100 μL per well in a 96-well plate, followed by adding EB-ICG-^{99m}Tc-HSA as 3, 0.3 or 0.03 nmole and then incubating this for 5 hrs. The viability of the DRO cells was not different with various concentrations (p>0.05); (B) Acute toxicity in the BALB/c mice. The test group of mice was intravenously injected with ten times higher than the optimal concentration (in vivo) in 50 μL of EB-ICG-^{99m}Tc-HSA (n=5) whereas the control mice were intravenously injected with 50 μL of saline (n=5). The body weight of mice was observed during 35 days, and no significant difference of the test group was observed as to the control group; (C) All the mice were sacrificed at the 35th day post EB-ICG-^{99m}Tc-HSA injection and the 6 tissues (lymph node, brain, heart, intestine, kidney and liver) were harvested and stained with H&E. No significant difference from the control group was observed.

First, the viability of luciferase expressing DRO cells barely showed differences with various concentrations of EB-ICG-^{99m}Tc-HSA in our vitro cellular toxicity study (Figure 6A). Similarly, acute toxicity was determined in the 10+ week old BALB/c mice. During a month, no significant behavior difference and body weight changes were observed in the EB-ICG-^{99m}Tc-HSA injected group as compared to that of the control group (Figure 6B). The organs from the sacrificed mice at the 35th day were stained with H&E, and the results showed no significant dissimilarity on comparison (Figure 6C).

Conclusion

We developed a new nano-sized triple modal SLN imaging agent called EB-ICG-^{99m}Tc-HSA. It is a very useful clinically and it showed a very ideal nature for SLN mapping. It enabled a high signal-to-noise ratio on the SLNs and it produced complementary triple modal signals with safety. As a result, it is an agent that promises to have positive clinical applications and it may have great advantages to complement the conventional single modal methods. This multimodal method could be beneficial for trainee or inexperienced surgeons to learn SLN surgery in early breast cancer.

Acknowledgments

This research was supported by the National Research Foundation of Korea (NRF) funded by the Ministry of Science, ICT & Future Planning (2014-030125). The authors declare that they have no conflicts of interest related to this study.

References

1. Noguchi M. Sentinel lymph node biopsy and breast cancer. *Br J Surg* 2002;89:21-34.
2. Krag D. Current status of sentinel lymph node surgery for breast cancer. *J Natl Cancer Inst* 1999;91:302-303.
3. Veronesi U, Paganelli G, Viale G, Luini A, Zurrida S, Galimberti V, Intra M, Veronesi P, Robertson C, Maisonneuve P, Renne G, De Cicco C, De Lucia F, Gennari R. A randomized comparison of sentinel-node biopsy with routine axillary dissection in breast cancer. *N Engl J Med* 2003;349:546-553.
4. Krag DN, Anderson SJ, Julian TB, Brown AM, Harlow SP, Costantino JP, Ashikaga T, Weaver DL, Mamounas EP, Jalovec LM, Frazier TG, Noyes RD, Robidoux A, Scarth HM, Wolmark N. Sentinel-lymph-node resection compared with conventional axillary-lymph-node dissection in clinically node-negative patients with breast cancer: overall survival findings from the NSABP B-32 randomised phase 3 trial. *Lancet Oncol* 2010;11:927-933.
5. Krag DN, Weaver DL, Alex JC, Fairbank JT. Surgical resection and radiolocalization of the sentinel lymph node in breast cancer using a gamma probe. *Surg Oncol* 1993;2:335-339.
6. Giuliano AE. Lymphatic mapping and sentinel node biopsy in breast cancer. *JAMA* 1997;277:791-792.
7. Sandrucci S, Casalegno PS, Percivale P, Mistrangelo M, Bombardieri E, Bertoglio S. Sentinel lymph node mapping and biopsy for breast cancer: a review of the literature relative to 4791 procedures. *Tumori* 1999;85:425-434.
8. Hung WK, Chan CM, Ying M, Chong SF, Mak KL, Yip AW. Randomized clinical trial comparing blue dye with combined dye and isotope for sentinel lymph node biopsy in breast cancer. *Br J Surg* 2005;92:1494-1497.
9. Sardi A, Spiegler E, Colandrea J, Frishberg D, Sing H, Regan P, Totoonchie A, Merchant D, Hochuli S, Setya V, Singer JA. The benefit of using two techniques for sentinel lymph node mapping in breast cancer. *Am Surg* 2002;68:24-28.
10. Kitai T, Inomoto T, Miwa M, Shikayama T. Fluorescence navigation with indocyanine green for detecting sentinel lymph nodes in breast cancer. *Breast Cancer* 2005;12:211-215.
11. McIntosh SA, Purushotham AD. Lymphatic mapping and sentinel node biopsy in breast cancer. *Br J Surg* 1998;85:1347-1356.
12. Wallace AM, Hoh CK, Limmer KK, Darrah DD, Schulteis G, Vera DR. Sentinel lymph node accumulation of lymphoseek and Tc-99m-sulfur colloid using a "2-day" protocol. *Nucl Med Biol* 2009;36:687-692.
13. Frangioni JV. In vivo near-infrared fluorescence imaging. *Curr Opin Chem Biol* 2003;7:626-634.
14. Lim YT, Kim S, Nakayama A, Stott NE, Bawendi MG, Frangioni JV. Selection of quantum dot wavelengths for biomedical assays and imaging. *Mol Imaging* 2003;2:50-64.
15. Zhang C, Wang S, Xiao J, Tan X, Zhu Y, Su Y, Cheng T, Shi C. Sentinel lymph node mapping by a near-infrared fluorescent heptamethine dye. *Biomaterials* 2009;31:1911-1917.
16. Jeong JM, Hong MK, Kim YJ, Lee J, Kang JH, Lee DS, Chung JK, Lee MC. Development of ^{99m}Tc-neomannosyl human serum albumin (^{99m}Tc-MSA) as a novel receptor binding agent for sentinel lymph node imaging. *Nucl Med Commun* 2004;25:1211-1217.
17. Dykewicz MS, Orfan NA, Sun W. In vitro demonstration of IgE antibody to folate-albumin in anaphylaxis from folic acid. *J Allergy Clin Immunol* 2000;106:386-389.
18. Bostick P, Essner R, Glass E, Kelley M, Sarantou T, Foshag LJ, Qi K, Morton D. Comparison of blue dye and probe-assisted intraoperative lymphatic mapping in melanoma to identify senti-

nel nodes in 100 lymphatic basins. *Arch Surg* 1999;134:43-49.
19. Krag D, Weaver D, Ashikaga T, Moffat F, Klimberg VS, Shriver C, Feldman S, Kusminsky R, Gadd M, Kuhn J, Harlow S, Beitsch P. The sentinel node in breast cancer - a multicenter validation study. *N Engl J Med* 1998;339:941-946.
20. Giuliano AE, Jones RC, Brennan M, Statman R. Sentinel lymphadenectomy in breast cancer. *J Clin Oncol* 1997;15:2345-2350.
21. Meyer-Rochow GY, Martin RC, Harman CR. Sentinel node biopsy in breast cancer: validation study and comparison of blue dye alone with triple modality localization. *ANZ J Surg* 2003; 73:815-818.
22. Morton DL, Wen DR, Wong JH, Economou JS, Cagle LA, Storm FK, Foshag LJ, Cochran AJ. Technical details of intraoperative lymphatic mapping for early stage melanoma. *Arch Surg* 1992;127:392-399.
23. Giuliano AE, Dale PS, Turner RR, Morton DL, Evans SW, Krasne DL. Improved axillary staging of breast cancer with sentinel lymphadenectomy. *Ann Surg* 1995;222:394-401.
24. Giuliano AE, Barth AM, Spivack B, Beitsch PD, Evans SW. Incidence and predictors of axillary metastasis in T1 carcinoma of the breast. *J Am Coll Surg* 1996;183:185-189.
25. Hardman R. A toxicologic review of quantum dots: toxicity depends on physicochemical and environmental factors. *Environ Health Perspect* 2006;114:165-172.
26. Shi C, Zhu Y, Cerwinka WH, Zhau HE, Marshall FF, Simons JW, Nie S, Chung LW. Quantum dots: emerging applications in urologic oncology. *Urol Oncol* 2008;26:86-92.
27. Raabe A, Beck J, Gerlach R, Zimmermann M, Seifert V. Near-infrared indocyanine green video angiography: a new method for intraoperative assessment of vascular flow. *Neurosurgery* 2003;52:132-139.
28. Tajima Y, Yamazaki K, Masuda Y, Kato M, Yasuda D, Aoki T, Kato T, Murakami M, Miwa M, Kusano M. Sentinel node mapping guided by indocyanine green fluorescence imaging in gastric cancer. *Ann Surg* 2009;249:58-62.
29. Tsujino Y, Mizumoto K, Matsuzaka Y, Niihara H, Morita E. Fluorescence navigation with indocyanine green for detecting sentinel nodes in extramammary Paget's disease and squamous cell carcinoma. *J Dermatol* 2009;36:90-94.
30. Bobin JY, Zinzindohoue C, Isaac S, Saadat M, Roy P. Tagging sentinel lymph nodes: a study of 100 patients with breast cancer. *Eur J Cancer* 1999;35:569-573.
31. Lim YT, Noh YW, Han JH, Cai QY, Yoon KH, Chung BH. Biocompatible polymer-nanoparticle-based bimodal imaging contrast agents for the labeling and tracking of dendritic cells. *Small* 2008;4:1640-1645.